Radiation Measurements 49 (2013) 95–102

Contents lists available at SciVerse ScienceDirect

Radiation Measurements

journal homepage: www.elsevier.com/locate/radmeas

Analysis of radiation dose variations measured by passive dosimeters onboard the International Space Station during the solar quiet period (2007–2008)

Satoshi Kodaira [a,*], Hajime Kawashima [a], Hisashi Kitamura [a], Mieko Kurano [a], Yukio Uchihori [a], Nakahiro Yasuda [a], Koichi Ogura [b], Ikuo Kobayashi [c], Akifumi Suzuki [c], Yasuhiro Koguchi [d], Yury A. Akatov [e], Vyacheslav A. Shurshakov [e], Raisa V. Tolochek [e], Tatiana K. Krasheninnikova [f], Anatoliy D. Ukraintsev [f], Elena A. Gureeva [g], Vladimir N. Kuznetsov [g], Eric R. Benton [h]

[a] National Institute of Radiological Sciences, Chiba, Japan
[b] Nihon University, Chiba, Japan
[c] Nagase Landauer Ltd., Ibaraki, Japan
[d] Chiyoda Technol Corporation, Ibaraki, Japan
[e] Institute of Biomedical Problems at Russian Academy of Sciences, Moscow, Russia
[f] OAO Biochimmash, Moscow, Russia
[g] Space Rocket Corporation Energia, Moscow Region, Russia
[h] Oklahoma State University, Stillwater, United States

HIGHLIGHTS

- We demonstrate the long-term dose variation by using passive detectors.
- Observed dose increase was due to the incremental increase in the altitude of the ISS.
- Trapped proton flux increase by the encounter during passage of the ISS through the SAA.
- Dose equivalent was increased due to the contribution of high LET components.
- A significant fraction was due to short-range recoil nuclei produced in target fragmentation reactions.

ARTICLE INFO

Article history:
Received 14 November 2011
Received in revised form
17 August 2012
Accepted 22 November 2012

Keywords:
Space radiation dosimetry
Passive detectors
Plastic nuclear track detector
Thermoluminescence detector
Long-term variation
Secondary particles
High LET particles
Target fragments

ABSTRACT

The average absorbed dose and dose equivalent rates from space radiation were observed using passive dosimeters with same material and configuration at the same location onboard the International Space Station (ISS) over four different occasions (I–IV) between 2007 and 2008. The passive dosimeters consisted of a combination of thermoluminescent detectors (TLDs) and plastic nuclear track detectors (PNTDs). Total average absorbed dose rate increased by 68 ± 9% over two years. The observed increase was due to the incremental increase in the altitude of the ISS over the course of the experiment and the corresponding increase in trapped proton flux encountered during passage of the ISS through the SAA (South Atlantic Anomaly), which was confirmed with the results monitored by DB-8 active dosimeter on the ISS. The PNTD data showed that the average absorbed dose and dose equivalent rates from particles of LET$_\infty$ $H_2O \geq 100$ keV/μm were 28 ± 2% and 51 ± 3% of ≥10 keV/μm during Periods I–III, while the dose contributions of particles ≥100 keV/μm during Period IV were 36 ± 5% and 59 ± 10%, respectively. The integral dose equivalent distribution during Period IV shows significant enhancement from particles ≥100 keV/μm. These facts suggest that a significant fraction of the high LET component is due to short-range recoil nuclei produced in target fragmentation reactions between primary protons and the nuclei of the passive dosimeters and surrounding materials.

1. Introduction

The measurement of absorbed dose and dose equivalent during manned space missions on the International Space Station (ISS) in low earth orbit (LEO) are important for evaluating the risk to

* Corresponding author. Radiation Measurement Research Section, National Institute of Radiological Sciences, 4-9-1 Anagawa, Inage, Chiba 263-8555, Japan. Tel.: +81 43 206 3479; fax: +81 43 206 3514.
E-mail address: koda@nirs.go.jp (S. Kodaira).

1350-4487/$ – see front matter © 2012 Elsevier Ltd. All rights reserved.
http://dx.doi.org/10.1016/j.radmeas.2012.11.020

astronaut health and safety. The radiation environment encountered during spaceflight is composed of a variety of different particles covering a wide range of energies. The principal contributions to radiation dose come from galactic cosmic rays (GCR) consisting mainly of protons and heavy ions up to iron with a peak energy of around 1 GeV/n, as well as lower energy protons and electrons in the Earth's radiation belts, and solar energetic particles (SEP) with energies up to several hundred MeV associated with coronal mass ejections (CME). The linear energy transfer, $LET_{\infty}H_2O$, of such particles ranges from ~0.1 to ~1000 keV/μm. The dose rates are constantly changing and depend mainly on the level of solar activity and on various spacecraft- and orbit-dependent parameters as the shielding distribution surrounding the detectors, location of the spacecraft within its orbit relative to the Earth, the attitude (orientation) and altitude changes. Consequently, continuous monitoring of dose rates is required to record and evaluate the personal radiation dose for crew members during spaceflight (Benton and Benton, 2001).

The radiation dose inside the ISS is continuously monitored using active detectors such as the NASA Johnson Space Center's Tissue Equivalent Proportional Counter (JSC-TEPC) (Badhwar et al., 1994) and the DB-8 dosimeters of the Russian Institute for Biomedical Problems (IBMP) (Markov et al., 2001). The DB-8 dosimeters are silicon detectors that operate independently at four locations within the ISS Russian Service Module. In addition to these active monitors, passive dosimeters consisting of thermoluminescent detectors (TLDs) and plastic nuclear track detectors (PNTDs) are used to measure integral absorbed dose and dose equivalent over periods on the order of 3–6 months and their results are combined to provide the primary dose of record for each ISS crew member (Nagamatsu et al., 2006; Zhou et al., 2007).

The combination method of radiation dose data measured by both TLD and PNTD permits easy and precise measurement of space radiation exposure aboard spacecraft (Doke et al., 1995). The passive dosimeters have the advantage of being small, lightweight, low cost and require no electric power, but are incapable of being read out in real time and provide no information on time variations in dose and dose equivalent rates in the dynamically changing space radiation environment. Analysis of several data sets obtained by passive dosimeters exposed for different durations makes it possible to estimate long-term variations of dosimetric quantities as a function of time. The analysis for obtaining time variations was carried out by means of the different types of passive detector at different locations inside ISS for over-lapping or discontinuous periods of time (Benton et al., 2002a; Ambrozova et al., 2011). The data set obtained by the same detector configuration at the same location over the long-term period allow us to observe the space radiation variation without any change in systematic parameters such as differences in detector type, location and orientation inside the spacecraft.

In this paper, we present variations in space radiation absorbed dose and dose equivalent rates measured by using passive dosimeters of the same type and configuration and at the same location over a two year period from 2007 to 2008.

2. Passive dosimeters

A combination of TLD-100 thermoluminescence detector (TLD) and HARZLAS TD-1 plastic nuclear track detector (PNTD) provides absorbed dose and dose equivalent measurements from all important space radiation sources and covers the whole energy range relevant to radiation protection in spaceflight. TLDs measure absorbed dose from energetic photons and charged particles over the whole LET spectrum, but register the dose from charged particles of $LET_{\infty}H_2O \geq 10$ keV/μm with less than 100% efficiency. PNTDs provide measurement of the LET spectrum, absorbed dose, and dose equivalent from charged particles of $LET_{\infty}H_2O \geq 10$ keV/μm. The data from the two types of detector were combined to yield values of total absorbed dose and total dose equivalent accumulated over the duration of the exposure (Benton et al., 2002a; Hajek et al., 2008; Tawara et al., 2011).

The TLD-100 (LiF:Mg,Ti), provided by Nagase Landauer Inc., Japan, was employed and analyzed by the standard processing protocol including annealing, read-out luminescence and quality control established by Nagase Landauer Inc. for personal dosimetry (NIRS report, 2009). The TLD-100 was calibrated by means of a standard ^{137}Cs γ-ray source and heavy ion beams from HIMAC (Heavy Ion Medical Accelerator in Chiba) at NIRS (National Institute of Radiological Sciences).

The PADC (poly allyl diglycol carbonate), so-called CR-39, HARZLAS TD-1, manufactured by Fukuvi Chemical Industry, Japan, was employed as the PNTD and was analyzed using a high speed imaging microscope (HSP-100) and nuclear track analysis software (PitFit) (Yasuda et al., 2005) after chemical etching for 8 h in 7 N NaOH solution at 70 °C. The amount of bulk etch was 13–15 μm. The area analyzed on each layer was 4–27 mm^2. The HARZLAS TD-1 detector can register nuclear tracks of charged particles with $LET_{\infty}H_2O \geq 5$ keV/μm (Ogura et al., 2001). HARZLAS TD-1 PNTD was calibrated by means of heavy ion beams of known LET obtained at the NIRS HIMAC. LET spectra, dose, and dose equivalent ≥10 keV/μm were obtained from the HARZLAS TD-1 PNTDs (NIRS report, 2009).

3. Experiment

3.1. Passive dosimeters onboard ISS

The multiple sets of TLD and PNTD were exposed in four sessions of varying duration between January 19, 2007 and October 24, 2008 in the Pirs-1 module attached to the Russian Service Module of the ISS. The details of the four exposure sessions (#1–#4) are summarized in Table 1. The same configuration of passive dosimeters was carried out in each session. Each detector set was installed at the same location in the Pirs-1 module such that the shielding distribution surrounding the detector sets was fairly constant over the duration of the experiment. The analysis of the four detector sets permitted us to determine the variation in absorbed dose and dose equivalent rates as a function of time. The upper panel in Fig. 1 shows the four sessions throughout the two year period. By subtracting the overlapping periods during the four sessions, the exposure durations were divided into four periods (I–IV) as shown in the lower panel of Fig. 1. Details of the division from four sessions to four periods are summarized in Table 2. Here, DOY (day of year) means the number of days since January 1, 2007. For example, DOY = 111 corresponds to April 21, 2007. There is an overlap of about two weeks between periods II and III. However it does not introduce significant error in dosimetric results for this analysis because the ratio of overlapping period to the total period is only about 7%.

Table 1
Exposure durations of the four sessions (#1–#4).

	Duration	Exposure days
Session #1	January 19, 2007–April 21, 2007	92
Session #2	January 19, 2007–October 22, 2007	276
Session #3	October 10, 2007–April 19, 2008	191
Session #4	October 10, 2007–October 24, 2008	380

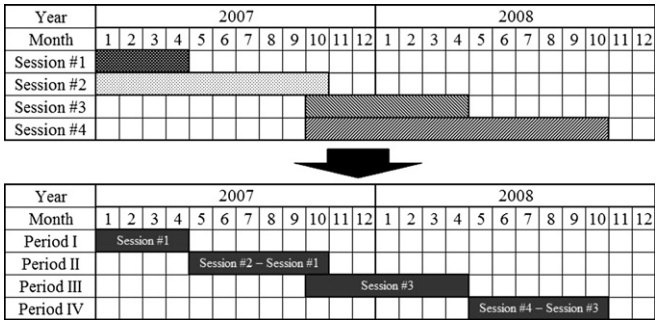

Fig. 1. Space experiment schedule of four sessions (#1–#4) between 2007 and 2008 and the four periods (I–IV) determined by subtracting overlapping times of the four experiment sessions (#1–#4).

3.2. Space radiation environment during 2007–2008

The variations in radiation dose and dose equivalent rates are related to the dependence of the radiation field on several environmental parameters and orbital parameters of the spacecraft. The space radiation field due to the primary cosmic rays depends on the solar activity. The change in solar activity over the course of the 11 year solar cycle has two effects on the space radiation environment encountered by the ISS. First, the frequency of solar particle events (SPE) associated with solar flares and CMEs is positively correlated with the level of solar activity. Second, the GCR intensity is negatively correlated with solar activity since the increased intensity of the solar wind associated with increased solar activity during solar maximum attenuates a greater fraction of the incident GCR flux arriving from the outer solar system. The two year period (2007–2008) during which the passive dosimeters were exposed aboard the ISS corresponded to the approach of solar minimum and the end of solar cycle 23. No significant solar flare or CME events exceeding X class occurred during the period of this work. The radiation environment in the ISS orbit was quiet and stable as indicated by the D_{st}, A_p and K_p indices used to characterize the magnitude of disturbance of the geomagnetic field (Mayaud, 1980). We conclude that solar particle events did not contribute to the variation of radiation dose rate observed in the passive dosimeter data.

The other parameters changing the space radiation field inside the ISS include the shielding distribution surrounding the detectors, the location of the ISS within its orbit relative to the Earth, and the attitude (orientation) and altitude of the ISS. The three dimensional shielding distribution surrounding a given location inside a spacecraft will affect the dose and dose equivalent rates measured at that location both by attenuating the overall flux of particles and by modifying the radiation field through the production of secondary particles in the shielding material. The passive dosimeters exposed during the four sessions of this experiment were all located in the same place in the Pirs-1 module. This fact, together with the fact that short-term variations in the shielding distribution due to the movement of equipment, personnel, etc. likely had only minimal effect over the long integration times of the passive dosimeter exposures, allows us to conclude that the shielding distribution surrounding the detectors is unlikely to be a significant contributor to the increase in dose and dose equivalent rates observed in the passive dosimeters over the course of the experiment. Because the radiation field in LEO is not isotropic, changes in the attitude of a spacecraft can result in changes to dose and dose equivalent rates measured at a given location within a LEO spacecraft. The two major sources of anisotropy in the LEO radiation field are 1) the shadow caused by the Earth, and 2) the East/West trapped proton anisotropy encountered when the spacecraft passes through the SAA. If a spacecraft maintains a fixed orientation with respect to the Earth while in LEO, these effects will have minimal influence on long-term dose and dose equivalent rates. During the two years of this experiment, the ISS orbited predominantly in the XVV attitude and the brief periods at different attitudes were distributed fairly uniformly over this duration. Based on these observations, it appears likely that changes in attitude of the ISS over the two year course of the experiment would have had little effect on the long-term variations in dose and dose equivalent rates. The dose dependency on the altitude is discussed separately in Sections 4. Results and 5. Discussion.

Table 2
Specification of dividing into four periods (I–IV) from the four sessions (#1–#4).

	DOY since Jan. 1, 2007	Dividing method
Period I	19–111	Period I = session 1
Period II	111–295	Period II = session 2–session 1
Period III	283–475	Period III = session 3
Period IV	475–663	Period IV = session 4–session 3

4. Results

The integral LET flux spectra for the four exposure periods (I–IV) measured by PNTDs are shown in Fig. 2. The average integral flux from particles of $LET_\infty H_2O \geq 10$ keV/μm increased slightly toward the latter half of 2008. In particular, the data for Period IV shows an enhancement in flux in the high LET region (>100 keV/μm).

The values of absorbed dose and dose equivalent measured by TLD and PNTD for each session (#1–#4) are shown in Table 3. The dose equivalent was obtained by applying the LET-dependent definition of the quality factor defined in ICRP-60 (ICRP, 1991). Since TLDs register the dose from charged particles of $LET_\infty H_2O \geq 10$ keV/μm with less than 100% efficiency, the total dose, covering the whole LET range of space radiation is obtained by combining data from TLDs (<10 keV/μm) with that from PNTDs (≥10 keV/μm) after subtracting that fraction from the TLD dose >10 keV/μm. The dose and dose equivalent rates for each period (I–IV), determined using the formulas listed in Table 2, are summarized in Table 4. The dose data for >100 keV/μm obtained from PNTDs are also shown. Table 5 summarizes the mean quality

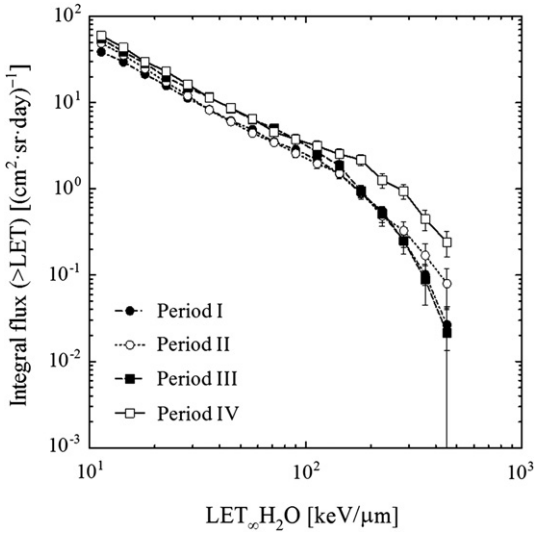

Fig. 2. Integral LET flux spectra for the four periods (I–IV) measured by PNTD.

Table 3
Absorbed dose and dose equivalent measured by TLD, PNTD and their combination for the four sessions (#1–#4). LET threshold of PNTD is 10 keV/μm.

	Absorbed dose measured by TLD [mGy]	Absorbed dose measured by PNTD [mGy]	Dose equivalent obtained by PNTD [mSv]	Total absorbed dose [mGy]	Total dose equivalent [mSv]
Session #1	20.7 ± 0.6	2.2 ± 0.1	28.7 ± 1.1	21.5 ± 0.6	48.0 ± 1.3
Session #2	70.9 ± 2.4	7.2 ± 0.2	86.0 ± 4.0	73.4 ± 2.4	152.2 ± 4.6
Session #3	56.3 ± 1.7	6.1 ± 0.2	78.0 ± 4.5	58.5 ± 1.7	130.3 ± 4.9
Session #4	127.7 ± 2.5	13.3 ± 0.4	164.6 ± 6.8	132.5 ± 2.5	283.9 ± 7.3

factors for total dose results (covering the whole LET range) and for particles of $LET_\infty H_2O \geq 10$ keV/μm and ≥100 keV/μm in the four periods (I–IV). The average total quality factor, Q_{Total}, for each period was found to be around 2.0, which is consistent with values obtained in previous space experiments (Benton et al., 2002a; Doke et al., 2001), while average Q values for high LET particles, especially $LET_\infty H_2O \geq 100$ keV/μm, decreased toward Period IV.

Fig. 3(a) and (b) shows the variations in absorbed dose and dose equivalent rates as a function of DOY between days 19 and 663, corresponding to January 19, 2007 and October 24, 2008. The data are presented in three ways: (1) average dose rate for $LET_\infty H_2O < 10$ keV/μm ($D_{<10\ keV/\mu m}$), (2) average dose and dose equivalent rate from particles of $LET_\infty H_2O \geq 10$ keV/μm ($D_{\geq 10\ keV/\mu m}$ and $H_{\geq 10\ keV/\mu m}$) and (3) total average dose and dose equivalent rates (D_{Total} and H_{Total}). Since the quality factor for $LET_\infty H_2O < 10$ keV/μm is defined as 1, $H_{<10\ keV/\mu m} = D_{<10\ keV/\mu m}$. The average dose rate as a function of DOY increased with time toward Period IV. D_{Total} during Period IV increased by 68 ± 9% above that measured during Period I.

5. Discussion

5.1. Comparison with DB-8 active dosimeters inside ISS

The absorbed dose rates measured by passive dosimeters were compared with the data measured by the DB-8 active dosimeter which uses Si detectors to monitor dose rate at four locations in the Russian Service Module of the ISS (Benghin et al., 2005; Lishnevskii et al., 2010). The DB-8 No. 1 is installed on the starboard side behind panel No. 410, which is near the Pirs-1 module where our passive dosimeters were located. The absorbed dose rate data obtained by DB-8 No. 1 (D_{DB-8}) (Lishnevskii et al., 2010) were compared to the results from passive dosimeters (D_{Total}) as a function of DOY in Fig. 4. The DB-8 data points (open triangle) are the average daily absorbed dose rate during the four periods. The average dose rate and its upward trend measured by the passive dosimeters as a function of time are generally in good agreement with the data measured by DB-8 No. 1. Lishnevskii et al. concluded that the gradual increase tendency of absorbed dose is due to the increase of trapped proton intensity due to ISS altitude change. However, DB-8 does not provide information on the particle LET spectrum. It is designed as the daily area dose monitor inside ISS and is only sensitive to ions of 0.2 keV/μm < $LET_\infty H_2O$ < 33 keV/μm (Benghin, 2011), which comprise ~97% of the space radiation charged particle spectrum. PNTDs provide detailed information on the LET spectrum between 10 and ~1500 keV/μm, allowing analysis of the high LET component.

5.2. Low LET contribution to dose rate increase

The major reason behind the increase in long-term average dose and dose equivalent rates over the two year course of this experiment is largely due to the overall increase in altitude of the ISS orbit over this time period and, specifically, the increase in altitude of the ISS during passage through the SAA (Badhwar et al., 1997; Badhwar et al., 1998; Badhwar, 2002; Akopova et al., 2007). Fig. 5 shows mean altitude of the ISS between 2007 and 2008 together with the average total absorbed dose rate (D_{total}). The average altitude (open down-triangles) was obtained by averaging daily mean ISS altitude (thin solid-line) over the four periods. The mean altitude was gradually increased from period I (341 km) to period IV (354 km), while the ISS altitude during period IV was drastically changed from 345 km at DOY = 477 to 365 km at DOY = 605. The highest altitude during this experiment was 365 km in the Period IV. The increase in average dose rate is in good agreement with the increase in average ISS altitude over the four periods of the experiment. The proportionally larger increase in dose rate versus altitude from Periods III to IV can be explained by the fact that dose rate rapidly increases with altitude inside the SAA, and is confirmed by the DB-8 results during the same period (Lishnevskii et al., 2010). The dose rate values determined using the AP8MIN trapped proton model (Armstrong and Colborn, 2000) are also shown in Fig. 5. The differential proton flux as a function of energy between 50 and 300 MeV was calculated at solar minimum for average ISS altitudes of 341–365 km. The absorbed dose for each proton was found by multiplying the differential flux at that energy by its corresponding value of $LET_\infty H_2O$ as determined by the SRIM range/energy code. The average absorbed dose rates integrated between 50 MeV and 300 MeV were obtained for the mean ISS altitudes during each period (I–IV) and at the highest altitude during Period IV. The calculated absorbed dose rate from trapped protons (D_{AP8}) is shown in Fig. 5 in the form of bold-dashed lines. The large difference in average dose rate between the average altitude (354 km) and maximum altitude (365 km) during Period IV

Table 4
Absorbed dose and dose equivalent rates for $LET_\infty H_2O < 10$ keV/μm, ≥10 keV/μm, ≥100 keV/μm and the total results for the four periods (I–IV). LET threshold of PNTD is 10 keV/μm.

	$LET_\infty H_2O < 10$ keV/μm	$LET_\infty H_2O \geq 10$ keV/μm		$LET_\infty H_2O \geq 100$ keV/μm		Total results (covering whole LET range)	
	$D_{<10\ keV/\mu m}$ ($H_{<10\ keV/\mu m}$) [μGy (μSv)/day]	$D_{\geq 10\ keV/\mu m}$ [μGy/day]	$H_{\geq 10\ keV/\mu m}$ [μSv/day]	$D_{\geq 100\ keV/\mu m}$ [μGy/day]	$H_{\geq 100\ keV/\mu m}$ [μSv/day]	D_{Total} [μGy/day]	H_{Total} [μSv/day]
Period I	225.0 ± 7.0	24.2 ± 0.6	311.8 ± 11.7	7.5 ± 0.4	169.7 ± 10.3	233.8 ± 7.0	521.4 ± 13.6
Period II	272.7 ± 13.3	27.2 ± 1.3	311.4 ± 22.4	7.3 ± 0.8	157.9 ± 19.7	282.2 ± 13.4	566.4 ± 26.1
Period III	294.6 ± 9.1	32.2 ± 1.3	408.3 ± 23.8	8.8 ± 1.4	202.2 ± 20.2	306.0 ± 9.2	682.1 ± 25.5
Period IV	379.7 ± 16.3	37.9 ± 2.5	461.0 ± 43.5	13.6 ± 1.8	272.1 ± 38.1	393.9 ± 16.4	816.9 ± 46.5

Table 5
Mean quality factors for total dose results (covering whole LET range) and for particles of LET$_\infty$H$_2$O ≥ 10 keV/μm and ≥100 keV/μm in the four periods (I–IV).

	Q_{Total} ($=H_{Total}/D_{Total}$)	$Q_{\geq 10\ keV/\mu m}$ ($=H_{\geq 10\ keV/\mu m}/D_{\geq 10\ keV/\mu m}$)	$Q_{\geq 100\ keV/\mu m}$ ($=H_{\geq 100\ keV/\mu m}/D_{\geq 100\ keV/\mu m}$)
Period I	2.2 ± 0.1	12.9 ± 0.6	22.6 ± 1.8
Period II	2.0 ± 0.1	11.4 ± 1.0	21.6 ± 3.6
Period III	2.2 ± 0.1	12.7 ± 0.9	23.0 ± 4.3
Period IV	2.1 ± 0.1	12.2 ± 1.4	20.0 ± 3.9

illustrates the effect of relatively large changes in ISS altitude while passing through the SAA.

5.3. High LET contribution to dose rate increase

Fig. 6 shows the average dose and dose equivalent rates from charged particles of LET$_\infty$H$_2$O ≥ 10 keV/μm and ≥100 keV/μm measured in PNTD for the four periods. The averaged absorbed dose rate and the dose equivalent rate from particles of LET$_\infty$H$_2$O ≥ 100 keV/μm are occupied with 28 ± 2% and 51 ± 3% of the ≥10 keV/μm particle contributions during the Period I–III, respectively. However, during Period IV, the dose contributions from ≥100 keV/μm particles are 36 ± 5% for D and 59 ± 10% for H of that from ≥10 keV/μm particles. On the other hand, as summarized in Table 5, the mean quality factor for high LET particles, especially $Q_{\geq 100\ keV/\mu m}$, decreased toward Period IV. One of the reasons is due to the increase of low LET particles as mentioned in 5.2. However, as shown in Fig. 7, the integral dose equivalent distribution of ≥100 keV/μm during Period IV lies significantly above that measured during Period III. The enhancement of high LET components of ≥100 keV/μm lead to the decrease of mean quality factor because Q as a function of LET as defined in ICRP-60 (ICRP, 1991) decreases above 100 keV/μm.

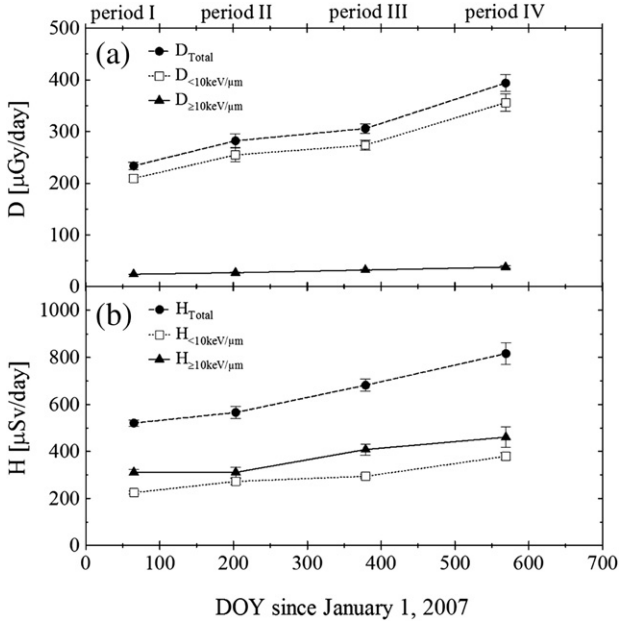

Fig. 3. Variations in (a) absorbed dose rate and (b) dose equivalent rate as a function of DOY between days 19 and 663, corresponding to January 19, 2007 and October 24, 2008. The data are presented in three ways: (1) average dose data for LET$_\infty$H$_2$O < 10 keV/μm (absorbed dose rate $D_{<10\ keV/\mu m}$ and dose equivalent dose rate $H_{<10\ keV/\mu m}$), (2) dose data for LET$_\infty$H$_2$O ≥ 10 keV/μm ($D_{\geq 10\ keV/\mu m}$ and $H_{\geq 10\ keV/\mu m}$) and (3) total dose data (D_{Total} and H_{Total}).

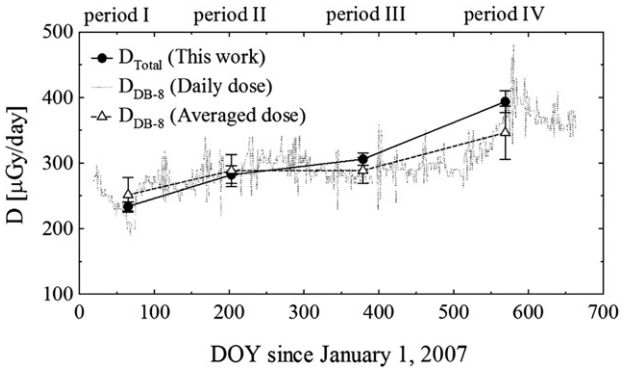

Fig. 4. Comparison of absorbed dose rates obtained by passive dosimeters (D_{Total}) and the DB-8 active dosimeter No. 1 (D_{DB-8}) as a function of DOY. DB-8 data points (open triangles) are the average daily absorbed dose rate during the four periods.

Since the maximum LET of a proton in water is ~95 keV/μm, average dose and dose equivalent rates from charged particles ≥100 keV/μm include only the contribution from particles of $Z \geq 2$. To evaluate dose variation of high LET components, we compared our results with GCR data (Public level 2 data of ACE/CRIS) obtained from the Cosmic Ray Isotope Spectrometer (CRIS) (Israel et al., 2005) instrument aboard the Advanced Composition Explorer (ACE) satellite for the same two year period. The ACE satellite provides information on GCR intensity free of geomagnetic effects, since it is located at the L1 Lagrange point, outside the geomagnetosphere. CRIS provides data on daily differential flux (F) for individual heavy elements of the GCR from B to Ni at energies below 500 MeV/n. The absorbed dose and dose equivalent from GCR were calculated using the CRIS data as follows:

(1) The GCR flux data as a function of Z between 3 and 28 and energy below 500 MeV/n were obtained from the CRIS online database (Public level 2 data of ACE/CRIS).
(2) The LET$_\infty$H$_2$O for individual nuclear charge and energy was calculated using the SRIM range/energy code (Ziegler and Biersack, 2003) and LET spectra were generated. LET$_\infty$H$_2$O ranged from approximately 10–400 keV/μm.
(3) The daily average absorbed dose rate (D_{ACE} [μGy/day]) was calculated by:

$$D_{ACE} = 1.602 \times 10^{-3} \cdot 4\pi T \sum_{Z,E} L(Z,E) \cdot F(Z,E) \cdot \Delta E$$

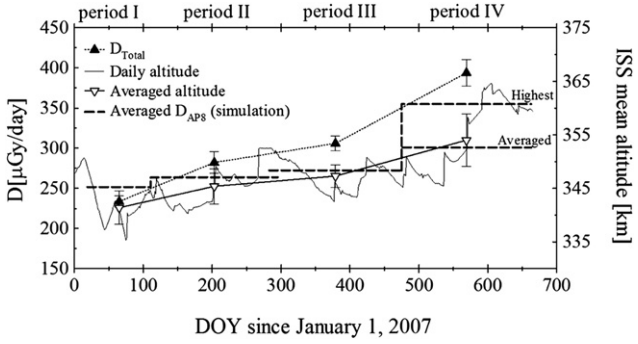

Fig. 5. Comparison of variations of mean ISS altitude with the average total absorbed dose data obtained from TLD and PNTD as a function of DOY. Average altitude (open down-triangles) was obtained by averaging daily mean ISS altitude (thin solid-line) during the four periods.

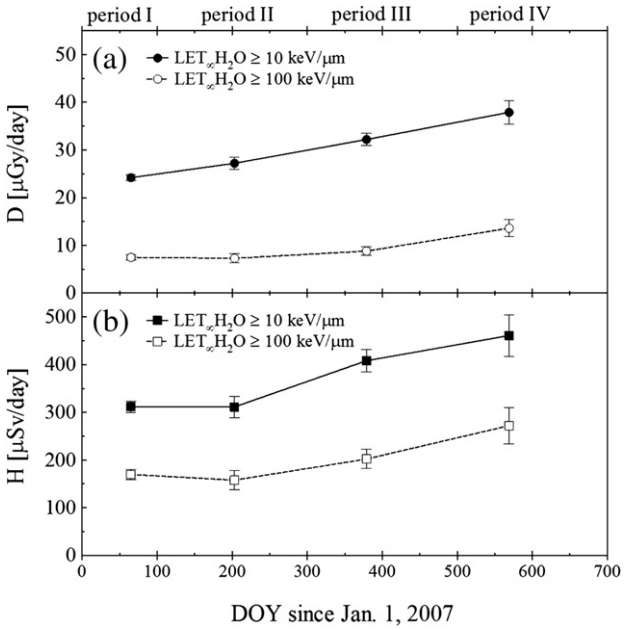

Fig. 6. Variations in (a) absorbed dose rate and (b) dose equivalent rate for $LET_\infty H_2O \geq 10$ keV/μm (closed circles and squares) and ≥100 keV/μm (open circles and squares), respectively.

where T (sec) denotes observation time, L (keV/μm) denotes $LET_\infty H_2O$ for a given nuclear charge (Z) and energy (E), F $(cm^2\ sr\ sec\ MeV/n)^{-1}$ denotes differential flux at (Z,E) and ΔE (MeV/n) denotes energy bin for a particular Z.

(4) The daily average dose equivalent, H_{ACE} (μSv/day), was obtained by:

$$H_{ACE} = 1.602 \times 10^{-3} \cdot 4\pi T \sum_{Z,E} L(Z,E) \cdot Q[L(Z,E)] \cdot F(Z,E) \cdot \Delta E$$

where $Q[L(Z,E)]$ is the LET-dependent quality factor defined in ICRP-60 (ICRP, 1991).

The absorbed dose and dose equivalent rate data from ACE/CRIS contains only the heavy charged particle component and does not include the contribution from protons and He, despite the fact that this latter component makes up ~97% of the GCR flux. Thus, it is most appropriate to compare the ACE/CRIS data with results from PNTDs which have a similar range of sensitivity in Z and E. Fig. 8 shows the average integral LET flux spectra obtained from the ACE/CRIS data, together with that measured by PNTDs aboard the ISS for the four periods of this experiment. The ACE/CRIS curves tend to flatten as LET decreases towards 10 keV/μm due to the fact the CRIS instrument is insensitive to protons, helium and relativistic energy heavy ions. In general, the ACE/CRIS spectra lie above the LET spectra measured in the PNTDs. In addition, there is less difference amongst the ACE/CRIS spectra for the four periods than amongst the PNTD spectra for the same exposure periods. However, during Period IV, the difference between the ACE/CRIS and PNTD curves is reduced as compared to the three earlier periods and for $LET_\infty H_2O \geq 300$ keV/μm, the PNTD curve actually lies above that obtained from the ACE/CRIS data.

Fig. 9 shows the comparison of the variations of (a) absorbed dose rate and (b) dose equivalent rate obtained from ACE/CRIS data and PNTD data for $LET_\infty H_2O \geq 10$ keV/μm normalized for Period I. The gradual increases in ACE/CRIS data by 14 ± 8% for dose rate and 12 ± 10% for dose equivalent rate from Periods I to IV indicate that GCR intensity was increasing due to the decrease in solar activity. However, the PNTD data show significantly larger increases in dose and dose equivalent rates of 57 ± 11% and 48 ± 15%, respectively. The proportionally larger increases and the steeper slopes of PNTD data compared to ACE/CRIS data over the two years of the experiment indicate that, at best, the increase in GCR intensity resulting from decreased solar activity can account for only a fraction of the increase in average dose and dose equivalent rates measured by the passive dosimeters.

The most likely source of such an enhanced high-LET component is short-range recoil nuclei produced in target fragmentation reactions of primary protons (and of secondary protons and neutrons) with the nuclei of the passive dosimeters and surrounding material (Benton et al., 1996, 2002b; Tawara et al., 2002). The high energy trapped protons encountered during passage of the ISS through the

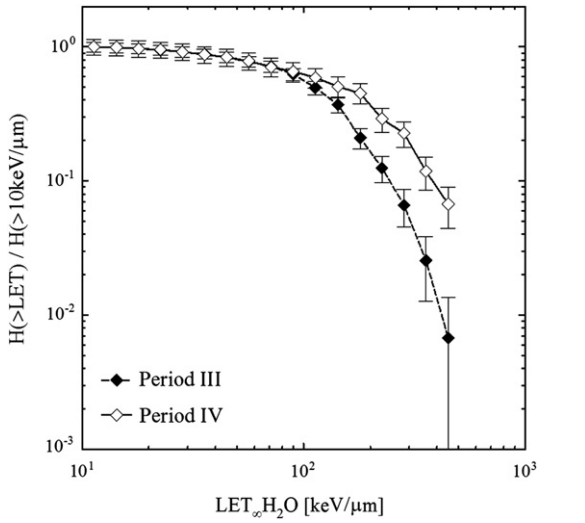

Fig. 7. Integral LET dose equivalent spectra for Period III and Period IV normalized to $LET_\infty H_2O \geq 10$ keV/μm.

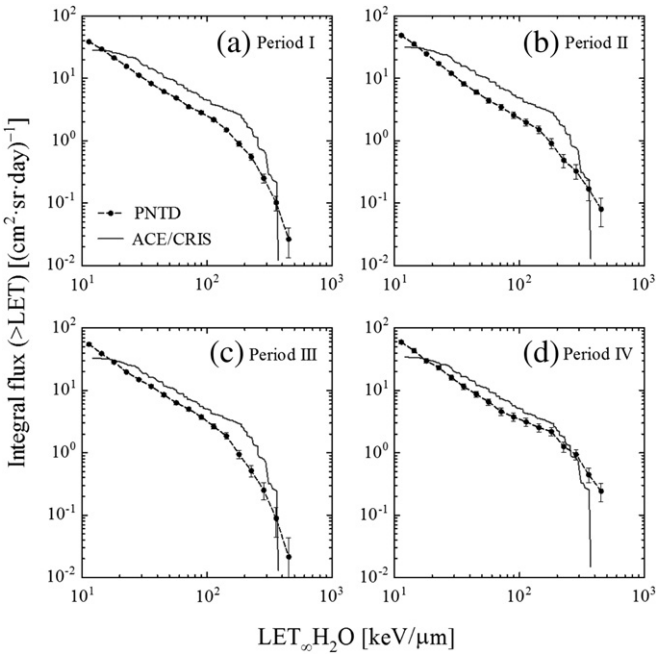

Fig. 8. Comparison of the average integral LET flux spectra obtained from the ACE/CRIS data with that measured in PNTD aboard ISS during the four periods (I–IV).

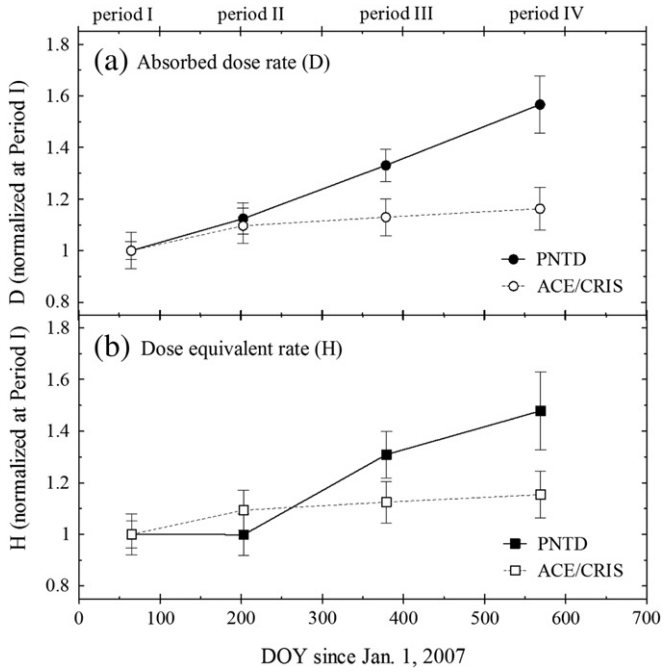

Fig. 9. Comparison of the variations of (a) absorbed dose rate and (b) dose equivalent rate obtained from ACE/CRIS data and PNTD data for LET$_\infty$H$_2$O $\geq$ 10 keV/μm normalized at Period I.

SAA interact with the structure of the ISS and its contents, including passive detectors and the bodies of the crew, producing secondary particles by target fragmentation reactions and resulting in the emission of protons, neutrons, and other light particles. Residual heavy recoil nuclei are left behind which are of high LET and short range due to their relatively large mass. The increase in ISS altitude to 365 km at DOY ~ 550 in Period IV brought the ISS into a more intense region of the SAA. The enhanced trapped proton flux in turn led to an increase in the number of target fragment interactions. The quantitative evaluation of average absorbed dose and dose equivalent rates, as well as mean quality factors, of such secondary charged particles will be investigated using precise measurement technology for short-range tracks by atomic force microscopy (Johnson et al., 2009).

6. Conclusions

We have demonstrated the use of passive dosimeters to measure long-term variations in average absorbed dose and dose equivalent rates that reflect changes in various environmental parameters. Absorbed dose and dose equivalent were measured using passive dosimeters of the same type and configuration at the same location onboard the ISS on four different occasions between 2007 and 2008. The variations in average dose and dose equivalent rate as a function of DOY show an increase toward Period IV. The total average absorbed dose rate for Period IV increased by 68 ± 9% over that measured for Period I. The average dose rate and its upward trend as a function of time measured by the passive dosimeters were generally in good agreement with the data measured by a DB-8 active dosimeter onboard the ISS except during Period IV. This increase was due to the incremental increase in the altitude of the ISS over the course of the experiment and the corresponding increase in trapped proton flux encountered during passage of the ISS through the SAA, which was confirmed with DB-8 results. The PNTD data show that the average absorbed dose and dose equivalent rates from particles of LET$_\infty$H$_2$O $\geq$ 100 keV/μm were 28 ± 2% and 51 ± 3% of that from ≥10 keV/μm particles during the Period I–III, respectively, while average absorbed dose and dose equivalent rate contributions from ≥100 keV/μm particles during Period IV were 36 ± 5% and 59 ± 10%, respectively. The integral dose equivalent distribution during Period IV shows significant enhancement above 100 keV/μm. These facts suggest that a significant fraction of high LET component is due to short-range recoil nuclei produced in target fragmentation reactions between primary protons and the nuclei of the passive dosimeters and surrounding materials. The quantitative evaluation of dose contribution due to such secondary particles will be investigated using the measurement technology of short range tracks in PNTD by atomic force microscopy.

Acknowledgements

We gratefully acknowledge the IBMP staff and the ISS crew for preparing, launching and recovering our detectors during the long duration of this experiment. We thank the ACE/CRIS instrument team and the ACE Science Center for providing the ACE data. This work was performed as a part of accelerator experiments of the Research Project at NIRS-HIMAC. We would like to express our thanks to the staff of NIRS-HIMAC for their kind support throughout the experiments for detector calibrations.

References

Akopova, A.B., Tatikyan, S.Sh., Manaseryan, M.M., Melkonyan, A.A., Ivanov, V.A., 2007. Investigation of radiation fields at different altitudes in near-Earth orbit. Adv. Space Res. 40, 1580–1585.
Ambrožová, I., Brabcová, K., Spurný, F., Shurshakov, V.A., Kartsev, I.S., Tolochek, R.V., 2011. Monitoring on board spacecraft by means of passive detectors. Radiat. Protect. Dosim. 144, 605–610.
Armstrong, T.W., Colborn, B.L., 2000. NASA contractor report; NASA CR-209879, TRAP/SEE Code Users Manual for Predicting Trapped Radiation Environments.
Badhwar, G.D., Cucinotta, F.A., Braby, L.A., Konradi, A., 1994. Measurements on the shuttle of the LET spectra of galactic cosmic radiation and comparison with radiation transport model. Radiat. Res. 139, 344–351.
Badhwar, G.D., Shurshakov, V.A., Tsetlin, V.V., 1997. Solar modulation of dose rate onboard the Mir station. IEEE Trans. Nucl. Sci. 44, 2529–2541.
Badhwar, G.D., Atwell, W., Cash, B., Petrov, V.M., Akatov, Yu.A., Tchernykh, I.V., Shurshakov, V.A., Arkhangelsky, V.A., 1998. Radiation environment on the Mir orbital station during solar minimum. Adv. Space Res. 22, 501–510.
Badhwar, G.D., 2002. Shuttle radiation dose measurements in the International Space Station orbits. Radiat. Res. 157, 69–75.
Benghin, V.V., Petrov, V.M., Kireeva, S.A., Markov, A.V., Volkov, A.N., Aleksandrin, A.P., Panasjuk, M.I., Kutuzov, J.V., Morozov, O.V., Teltsov, M.V., 2005. Analysis of radiation dose increases caused by solar cosmic ray events observed by the radiation monitoring system on the Russian segment of the International Space Station. Adv. Space Res. 36, 1749–1752.
Benghin, V.V., 2011. Private Communications.
Benton, E.R., Benton, E.V., Frank, A.L., Frigo, L.A., Csige, I., 1996. Secondary particle contribution to LET spectra on LDEF. Radiat. Meas. 26, 793–797.
Benton, E.R., Benton, E.V., 2001. Space radiation dosimetry in low-Earth orbit and beyond. Nucl. Inst. Meth. B184, 255–294.
Benton, E.R., Benton, E.V., Frank, A.L., 2002a. Passive dosimetry aboard the Mir Orbital Station: internal measurements. Radiat. Meas. 35, 439–455.
Benton, E.R., Benton, E.V., Frank, A.L., 2002b. Passive dosimetry aboard the Mir Orbital Station: external measurements. Radiat. Meas. 35, 457–471.
Doke, T., Hayashi, T., Nagaoka, S., Ogura, K., Takeuchi, R., 1995. Estimation of dose equivalent in STS-47 by a combination of TLDs and CR-39. Radiat. Meas. 24, 75–82.
Doke, T., Hayashi, T., Kikuchi, J., Sakaguchi, T., Terasawa, K., Yoshihira, E., Nagaoka, S., Nakano, T., Takahashi, S., 2001. Measurements of LET-distribution, dose equivalent and quality factor with the RRMD-III on the Space Shuttle Missions STS-84, -89 and -91. Radiat. Meas. 33, 373–387.
Hajek, M., Berger, T., Vana, N., Fugger, M., Pálfalvi, J.K., Szabó, J., Eördögh, I., Akatov, Y.A., Arkhangelsky, V.V., Shurshakov, V.A., 2008. Convolution of TLD and SSNTD measurements during the BRADOS-1 experiment onboard ISS (2001). Radiat. Meas. 43, 1231–1236.
ICRP, 1991. International Commission on Radiological Protection. The 1990 Recommendations of the ICRP, ICRP Publication 60, Annals of the ICRP, 21, Pergamon Press, New York.
Israel, M.H., Binns, W.R., Cummings, A.C., Leske, R.A., Mewaldt, R.A., Stone, E.C., Rosenvinge, T.T.von, Wiedenbeck, M.E., 2005. Isotopic composition of cosmic rays: results from the cosmic ray Isotope Spectrometer on the ACE spacecraft. Nucl. Phys. A758, 201c–208c.

Johnson, C.E., Benton, E.R., Yasuda, N., Benton, E.V., 2009. Analysis of short-range tracks and large track fluences in CR-39 PNTD using atomic force microscopy. Radiat. Meas. 44, 742–745.

Lishnevskii, A.E., Panasyuk, M.I., Benghin, V.V., Petrov, V.M., Volkov, A.N., Nechayev, O.Yu, 2010. Variations of radiation environment onboard the ISS in the year 2008. Cosmic Res. 48, 206–210.

Markov, A.V., Gribachev, K.G., Lyagushin, V.I., Volkov, A.N., Aleksandrin, A.P., Germantsev, Yu.L., Basov, Yu.Yu., Panasyuk, M.I., Kolesov, G.Ya, Tel'tsov, M.P., Belyaev, A.A., Kalinin, D.V., Myasnikov, A.G., Kutuzov, Yu.V., Persikov, M.B., Biryukov, A.S., Akulin, A.I., Petrov, V.M., Benghin, V.V., Shurshakov, V.A., 2001. Results of Measurements Obtained in the First Phase of the Radiation Monitoring System Deployment on the Russian Segment of the International Space Station. The 6th Workshop on radiation monitoring of the ISS (WRMISS), Oxford, UK, Sepp. 3–5.

Mayaud, P.N., 1980. Derivation, Meaning and Use of Geomagnetic Indices, Geophysical Monograph 22. Am. Geophys. Union, Washington D.C. NOAA National Geophysical Data Center. Geomagnetic Indices Bulletin, Data: http://www.ngdc.noaa.gov/stp/geomag/indices.html.

Nagamatsu, A., Masukawa, M., Kamigaichi, S., Kumagai, H., Masaki, M., Yasuda, N., Yasuda, H., Benton, E., Takayoshi H., Tawara, J., 2006. Development of the Space Radiation Dosimetry System 'PADLES'. Proc. 20th Workshop on Radiation Detectors and Their Uses, KEK proceeding 2006–7, 26–36.

NIRS report (NIRS R 62), 2009. Scientific Reports of Space Experiments (IBMP-NIRS-1 to 4) in the IBMP-NIRS Collaboration. National Institute of Radiological Sciences. Aug. 2009.

Ogura, K., Asano, M., Yasuda, N., Yoshida, M., 2001. Properties of TNF-1 track etch detector. Nucl. Instr. Meth. B185, 222–227.

Public level 2 data of ACE/CRIS: http://www.srl.caltech.edu/ACE/ASC/level2/.

Tawara, H., Doke, T., Hayashi, T., Kikuchi, J., Kyan, A., Nagaoka, S., Nakano, T., Takahashi, S., Terasawa, K., Yoshihira, E., 2002. LET distributions from CR-39 plates on Space Shuttle missions STS-84 and STS-91 and a comparison of the results of the CR-39 plates with those of RRMD-II and RRMD-III telescopes. Radiat. Meas. 35, 119–126.

Tawara, H., Masukawa, M., Nagamatsu, A., Kitajo, K., Kumagai, H., Yasuda, N., 2011. Characteristics of Mg_2SiO_4:Tb (TLD-MSO-S) relevant for space radiation dosimetry. Radiat. Meas. 46, 709–716.

Yasuda, N., Namiki, K., Honma, Y., Umeshima, Y., Marumo, Y., Ishii, H., Benton, E.R., 2005. Development of a high speed imaging microscope and new software for nuclear track detector analysis. Radiat. Meas. 40, 311–315.

Zhou, D., Semones, E., Gaza, R., Weyland, M., 2007. Radiation measured with passive dosimeters in low Earth orbit. Adv. Space Res. 40, 1575–1579.

Ziegler, J.F., Biersack, J.P., 2003. Computer Code SRIM2003, The Stopping and Range of Ions in Matter.